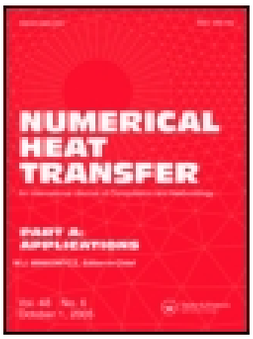

Taylor & Francis
Taylor & Francis Group

Numerical Heat Transfer, Part A: Applications

ISSN: 1040-7782 (Print) 1521-0634 (Online) Journal homepage: www.tandfonline.com/journals/unht20

Interaction of Surface Radiation with Conduction and Convection from a Vertical Channel with Multiple Discrete Heat Sources in the Left Wall

C. Gururaja Rao

To cite this article: C. Gururaja Rao (2007) Interaction of Surface Radiation with Conduction and Convection from a Vertical Channel with Multiple Discrete Heat Sources in the Left Wall, Numerical Heat Transfer, Part A: Applications, 52:9, 831-848, DOI: 10.1080/10407780701348257

To link to this article: https://doi.org/10.1080/10407780701348257

Numerical Heat Transfer, Part A, 52: 831–848, 2007

ISSN: 1040-7782 print/1521-0634 online
DOI: 10.1080/10407780701348257

Taylor & Francis
Taylor & Francis Group

INTERACTION OF SURFACE RADIATION WITH CONDUCTION AND CONVECTION FROM A VERTICAL CHANNEL WITH MULTIPLE DISCRETE HEAT SOURCES IN THE LEFT WALL

C. Gururaja Rao
Department of Mechanical Engineering, National Institute of Technology (Deemed University), Warangal, (A.P.), India

This article reports the results of a numerical study of the problem of interaction of surface radiation with conduction and convection from a vertical channel equipped with three flush-mounted discrete heat sources in the left wall. The governing equations for temperature distribution along each of the two channel walls have been deduced based on appropriate energy balance between various energy interactions in which the channel is involved. Radiosity-irradiation formulation is employed to tackle radiation-related calculations, with the view factors involved therein obtained using Hottel's crossed-string method. The governing nonlinear partial differential equations are converted into algebraic form through a finite-volume-based finite-difference method, and are subsequently solved using Gauss-Seidel iterative technique. An optimum grid system, with 26 grids along each of the three discrete heat sources and 11 grids along each of the two non-heat source portions of the board, is used for discretization of the computational domain. The effects of various pertinent parameters, viz., aspect ratio, volumetric heat generation, thermal conductivity, surface emissivity, and convection heat transfer coefficient, on temperature distribution along the left board, maximum temperature in the channel, and relative contributions of convection and surface radiation to heat dissipation from the channel are probed.

INTRODUCTION

Literature in the area of heat transfer has a major share pertaining to multimode heat transfer studies. The above kind of studies probably started with Zinnes [1], who worked on a vertical, heat-conducting, flat plate of finite thickness with an arbitrary heating distribution on its surface involved in laminar natural convection. This was a two-mode heat transfer study only, with researchers later picking up from there and extending their works to three-mode heat transfer problems, with interplay between surface radiation and convection (free, forced or mixed) in effecting heat dissipation from bodies with conduction and with (or without) uniform (or discrete) heat generation. A few of such studies include those of Tewari and Jaluria [2], Gorski and Plumb [3], Kishinami et al. [4], Cole [5], Mendez and Trevino [6], Dehghan and

Received 21 May 2006; accepted 27 February 2007.
Address correspondence to C. Gururaja Rao, Department of Mechanical Engineering, National Institute of Technology (Deemed University), Warangal 506 004 (A.P.), India. E-mail: cgr_gcr@yahoo.co.in

NOMENCLATURE

e	surface emissivity of each of the two channel walls	x_i	distance of the ith element from the leading edge of the channel wall, m
F_{ij}	view factor of an element i with reference to another element j of an enclosure	δ_c	convergence criterion, in percentage, $\lvert(T_{new} - T_{old})/T_{new}\rvert \times 100\%$
h	convection heat transfer coefficient, W/m^2 K	Δx	height of the wall element in the heat source portion, m
J_i	Radiosity of an element i of the enclosure, W/m^2	Δxo	height of the wall element in non-heat source portion, m
k	thermal conductivity of the channel walls and heat source, W/m K	σ	Stefan-Boltzmann constant ($=5.6697 \times 10^{-8}$ $W/m^2 K^4$)
L, t	height (or length) and thickness of each wall of the channel, m	**Subscripts**	
L_h	height (or length) of each of the three discrete heat sources, m	cond, in	conduction heat transfer into an element
q_v	volumetric heat generation in each heat source, W/m^3	cond, out	conduction heat transfer out of an element
S	spacing between the two walls of the channel or channel width, m	conv	convection heat transfer from an element
T	temperature at any location along the channel wall, K or °C	i	any arbitrary element of the channel wall
T_{max}	maximum temperature in the channel, K or °C	rad	heat transfer by surface radiation from an element
T_∞	ambient temperature of the fluid, K or °C	new, old	temperatures from current and previous iterations, respectively

Behnia [7], Gururaja Rao et al. [8–12], Gururaja Rao [13, 14], Bianco et al. [15], Slimi et al. [16], Borjini et al. [17], Hsu and Tan [18], Baek et al. [19], and Lee et al. [20].

A probe into the above literature reveals that the problem of the effect of surface radiation on conjugate convection from a vertical parallel-plate channel, provided with multiple, flush-mounted, discrete heat sources in one of its walls, has not been adequately looked into. On account of this, the present article aims at studying interplay between the multiple modes of heat transfer in the above geometry.

MATHEMATICAL FORMULATION AND METHOD OF SOLUTION

Figure 1 shows the schematic of the problem geometry considered in the present study. It consists of a vertical parallel-plate channel, possessing two plates, each of height L and thickness t, with the dimension perpendicular to the plane of paper taken to be unity. The left wall consists of three flush-mounted discrete heat sources, each of height L_h and thickness t. Each discrete heat source has heat generation in it at q_v W/m^3. The thermal conductivity of the board as well that of the three heat sources is taken to be identical and equal to k. The left wall has one heat source located at the channel entry, the second positioned at the channel exit, while the third is provided at the center. The surface emissivity of the inner surface of each channel wall is e. The right channel wall does not possess any heat source, while it has the

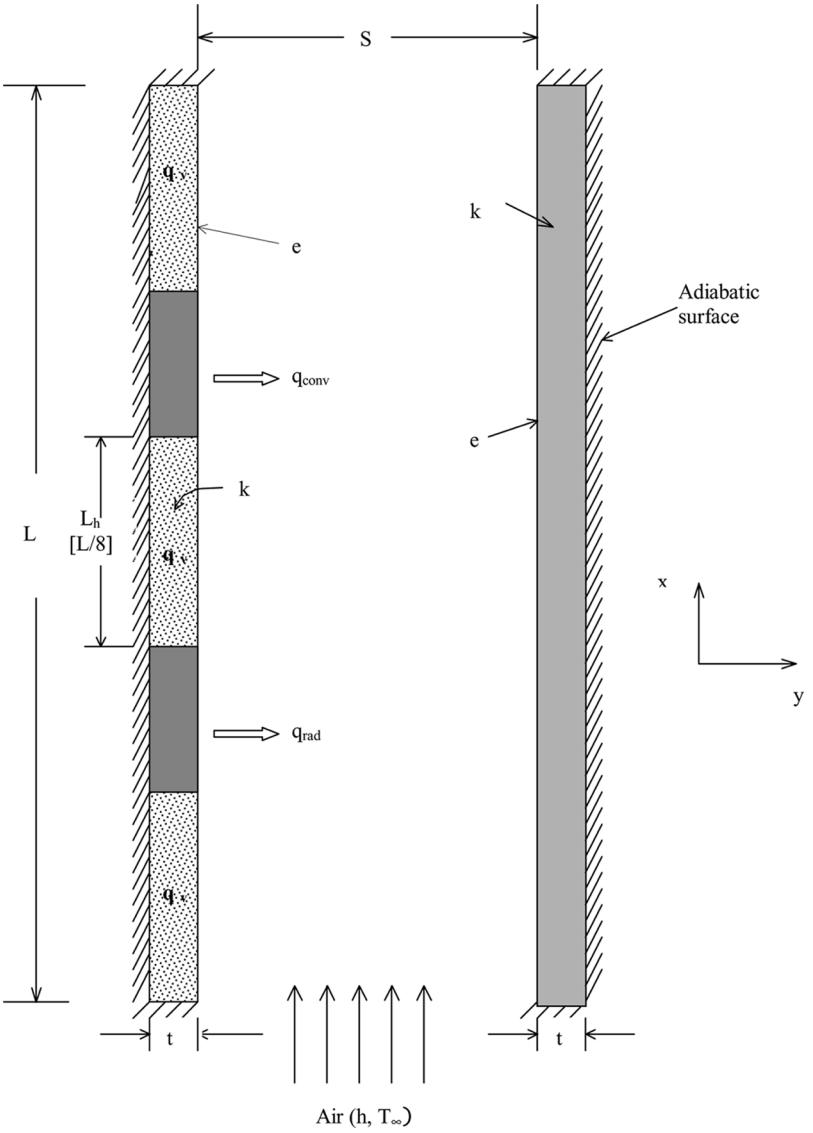

Figure 1. Schematic of the problem geometry chosen for the present study.

same conductivity (k) as the left wall. It merely receives heat from the left wall, which is conducted through it, before being subsequently dissipated by convection and radiation from its inner surface into the ambient.

The left, top, and bottom surfaces of the left wall and the right, top, and bottom surfaces of the right wall are adiabatic, implying the occurrence of heat exchange only within the channel. The spacing between the two channel walls (S) could be varied, and, in this context, an aspect ratio (AR) is defined as L/S. Obviously, with the wall height fixed at L, a larger aspect ratio implies a narrow channel

spacing, while toward smaller aspect ratios, the walls move farther apart. Air, a radiatively nonparticipating medium, is taken to be the cooling agent, with its temperature taken to be T_∞, while h is the convection heat transfer coefficient offered by the fluid vis-à-vis the surfaces of the walls of the channel.

In order to obtain the governing equations for temperature distribution along each of the two channel walls, typical elements are considered, and an energy balance is applied for various energy interactions in which the elements are involved Radiosity-irradiation formulation [21] is employed to tackle the radiation heat transfer calculations, while the view factor calculation is made using the crossed-string method of Hottel [22]. For example, considering an element within the central discrete heat source and performing an energy balance on various interactions pertaining to that element, one gets

$$q_v t\,\Delta x + q_{\text{cond, in}} = q_{\text{cond, out}} + q_{\text{conv}} + q_{\text{rad}} \tag{1}$$

This equation, after the substitution of all the relevant expressions and subsequent simplification, turns out to be

$$q_v t\,\Delta x + kt\left(\frac{\partial^2 T}{\partial x^2}\right)_i \Delta x = h\,\Delta x(T_i - T_\infty) + \frac{e}{(1-e)}(\sigma T_i^4 - J_i)\Delta x \tag{2}$$

where J_i refers to the radiosity of the element i, which is given by

$$J_i = e\sigma T_i^4 + (1-e)\sum_{j=1}^{n} F_{ij}J_j \qquad \text{for } 1 \le i \le n \tag{3}$$

where F_{ij} is the view factor from the ith element to the jth element of the enclosure, encompassing a total of n elements.

Similarly, by making appropriate energy balance on various elements along the left channel wall, viz., the element in the non-heat source portions, at the interface between heat source and non-heat source portions, top and bottom adiabatic ends of the wall, the pertinent equations for temperature distribution are obtained.

For the element in the non-heat source portion (where there is no heat generation), on making energy balance,

$$q_{\text{cond, in}} = q_{\text{cond, out}} + q_{\text{conv}} + q_{\text{rad}} \tag{4}$$

After substituting relevant expressions and simplifying,

$$kt\left(\frac{\partial^2 T}{\partial x^2}\right)_i \Delta x = h\,\Delta x(T_i - T_\infty) + \frac{e}{(1-e)}(\sigma T_i^4 - J_i)\,\Delta x \tag{5}$$

For the element at the interface between any one of the heat sources and the non-heat source portion, the energy balance results in

$$q_v t\left(\frac{\Delta x}{2}\right) + q_{\text{cond,in}} = q_{\text{cond,out}} + q_{\text{conv}} + q_{\text{rad}} \tag{6}$$

The above, after the appropriate mathematical manipulation, gives

$$q_v t\left(\frac{\Delta x}{2}\right) + kt\left(\frac{\partial^2 T}{\partial x^2}\right)_i \left(\frac{\Delta x + \Delta xo}{2}\right) = h\left(\frac{\Delta x + \Delta xo}{2}\right)(T_i - T_\infty) + \frac{e}{(1-e)}(\sigma T_i^4 - J_i)\left(\frac{\Delta x + \Delta xo}{2}\right) \tag{7}$$

For the element at the bottom adiabatic end of the left channel wall, the temperature variation follows the relation

$$q_v t\left(\frac{\Delta x}{2}\right) = q_{\text{cond,out}} + q_{\text{conv}} + q_{\text{rad}} \tag{8}$$

This finally results in

$$q_v t\left(\frac{\Delta x}{2}\right) = -kt\left(\frac{\partial T}{\partial x}\right)_i \left(\frac{\Delta x}{2}\right) + h\left(\frac{\Delta x}{2}\right)(T_i - T_\infty) + \frac{e}{(1-e)}(\sigma T_i^4 - J_i)\left(\frac{\Delta x}{2}\right) \tag{9}$$

Likewise, the governing equation for the temperature of the top adiabatic end of the left wall is also obtained. Further, for the right channel wall, which, as can be seen from Figure 1, does not possess any heat source, the energy balance for a typical element gives

$$q_{\text{cond,in}} = q_{\text{cond,out}} + q_{\text{conv}} + q_{\text{rad}} \tag{10}$$

This gives rise to

$$kt\left(\frac{\partial^2 T}{\partial x^2}\right)_i \Delta x = h\ \Delta x(T_i - T_\infty) + \frac{e}{(1-e)}(\sigma T_i^4 - J_i)\Delta x \tag{11}$$

For the top and bottom adiabatic ends of the right wall too, the governing equations for temperature distribution are evolved in a similar fashion.

The governing equations for temperature distribution, obtained as above, are in the form of nonlinear partial differential equations. They are converted into algebraic form through finite-volume-based finite-difference formulation and are subsequently solved simultaneously using Gauss-Seidel iterative procedure. A very stringent convergence criterion (δ_c) of 10^{-8} has been imposed on temperature, while full relaxation, with relaxation parameter equal to 1, is used during iterations. The temperatures along each of the two channel walls come out of the solution, which are subsequently used for obtaining the other results, such as peak channel

temperature (T_{max}), and relative contributions of convection and radiation to heat dissipation in the channel.

The height (L) of each channel wall is fixed to be 20 cm and the thickness (t) of the wall is 1.5 mm, while each of the three discrete heat sources is of height, $L_h = L/8$ or 2.5 cm. The various other parameters concerning the problem are chosen encompassing a very wide range for each of them. The aspect ratio (AR) is varied from 1 to 20, simulating a widely spaced channel to a narrowly spaced channel. The thermal conductivity (k) of the heat source as well as the board is varied from 0.25 to 1 W/m K, keeping in mind that electronic boards typically possess a thermal conductivity of the order of unity. The surface emissivity (e) of the board is varied from 0.05 to 0.85, in view of the fact that poor emitters (good reflectors) and good emitters (poor reflectors) typically possess surface emissivities of 0.05 and 0.85, respectively. The range for convection heat transfer coefficient (h) is taken to be from $5\,W/m^2\,K$ (free-convection-dominant regime) to $100\,W/m^2\,K$ (forced-convection-dominant regime).

RESULTS AND DISCUSSION

Before carrying out a detailed parametric study on the present problem, an optimum grid system that suits the entire range of parameters mentioned in the previous section is arrived at. Subsequently, this grid system is employed for all the remaining calculations of the current study.

Grid Convergence Test

In order to freeze on the optimum grid system for the present study, a detailed grid convergence test has been performed for a standard set of parameters, viz., $q_v = 10^6\,W/m^3$, $k = 0.25\,W/m\,K$, $h = 25\,W/m^2\,K$, $e = 0.45$, and $AR = 12$. The convergence of solution is tested in two phases. In the first phase, the number of grids in the non-heat source portion of the board is fixed at 11, while the number of grids along each heat source portion is varied. Table 1 shows the results of the above study. It may be seen that the peak channel temperature (T_{max}) changes by 0.0128% as the number of grids in each heat source is increased from 21 to 26, while the change in T_{max} is 0.0513% with a further increase in the grid number along the heat source to 31. The table also indicates a convergence in the solution for a grid

Table 1. Phase I of grid convergence test[a]

S. no.	Number of grids along each heat source	T_{max} (°C)	Percentage change (abs.)
1	11	78.00	—
2	16	77.97	0.0384
3	21	77.95	0.0256
4	26	77.96	0.0128
5	31	77.92	0.0513

[a]Number of grids along non-heat source portion fixed at 11, number of grids along each of the three heat sources varied.

Table 2. Phase II of grid convergence test[a]

S. no.	Number of grids along each non-heat source portion	T_{max} (°C)	Percentage change (abs.)
1	5	78.08	—
2	11	78.09	0.0014
3	16	78.09	0.0128

[a]Number of grids along each heat source fixed at 26, number of grids along non-heat source portion varied.

number of 26. In view of this, the number of grids along each discrete heat source is fixed to be 26.

In the second phase, fixing the number of grids in each source to be 26 as obtained above, the number of grids in each of the two non-heat source portions is varied. Table 2 shows the results of the above study. The table reveals that a change in the grid number in each non-heat source portion from 5 to 11 changes T_{max} by 0.0014%, while a further increase in the grid number to 16 changes T_{max} by 0.0128%. On account of this, the number of grids in each non-heat source portion is fixed to be 11.

Thus, all the subsequent calculations of the present study are performed by taking 26 grids and 11 grids, respectively, along each of the three heat sources and each of the two non-heat source portions.

Check for Energy Balance

A comprehensive check for energy balance has been made for testing the results of the present study for various arbitrarily chosen sets of input parameters. For example, for the case with $q_v = 10^5\,\mathrm{W/m^3}$, $k = 0.25\,\mathrm{W/m\,K}$, $h = 5\,\mathrm{W/m^2\,K}$, $e = 0.45$, and $\mathrm{AR} = 12$, using a grid size as finalized in the preceding section, the discrepancy between heat generated and heat dissipated has been found to be 0.051%. Various other sets of input parameters too yielded similar kind of results.

Validation

For validating the results of the present study, the code written for solving the current problem is run for the asymptotic limiting case, where the first and the last discrete heat sources have no heat generation, rendering the geometry to simulate a vertical channel with a single flush-mounted discrete heat source in its wall. The present author has already solved a problem of similar kind (see [10]). There has been a decent agreement between the two results for different sets of input parameters chosen for comparison, with maximum deviation restricted to about $\pm 1.51\%$. This acts as a good validation for the results of the present study.

Variation of Local Temperature along the Left and Right Channel Walls

Figure 2 shows the variation of the local temperature along the left (L) and right (R) walls of the channel, for $q_v = 10^6\,\mathrm{W/m^3}$, $k = 0.25\,\mathrm{W/m\,K}$, $h = 5\,\mathrm{W/m^2\,K}$,

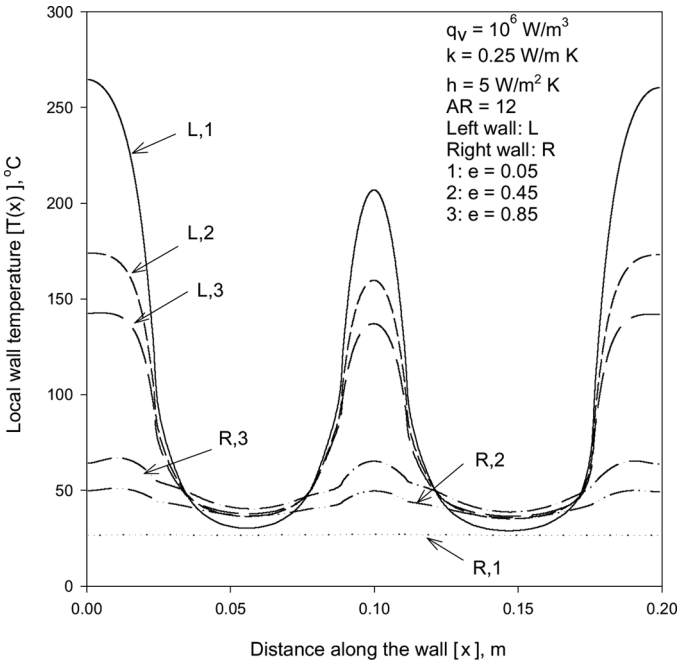

Figure 2. Variation of local temperature along the left and right channel walls for different emissivities.

and AR = 12, for three typical values of surface emissivity (e), 0.05, 0.45, and 0.85. The figure shows that the left wall temperature, for $e = 0.05$, decreases from the channel entry gradually until it reaches a minimum somewhere midway in the non-discrete heat source portion between the first and second heat sources. Owing to the fact that the second heat source will be following now, the wall temperature again starts increasing until it reaches a local maximum at the center of the central heat source. A mirror-image variation is noticeable in the top half of the left channel wall. It is to be noted that the above local maximum is less than the peak left wall temperature ($T_{\max}$), prevailing at the entry as well as at the exit of channel. With regard to the right wall, for the same emissivity (e) = 0.05, since the surface emissivity is very small and since there are no heat sources in it, not much appreciable variation is seen in the temperature distribution, though its temperature hovers around about 26.5°C along the wall. As emissivity increases, the left wall temperature variation continues to show similar trends as with first case ($e = 0.05$) discussed above, though for a given location along the wall, the temperature is seen to decrease with emissivity. This is owing to enhanced rate of radiation heat transfer from the left wall. The effect of emissivity (e) on right wall temperature distribution starts becoming apparent only toward larger values of e. Here, the temperature of the right wall undergoes comparatively significant variations, apparently due to continuous change in the radiation energy the wall receives from the left wall, which, in turn, is due to the presence of discrete heat sources along the left wall. To quantify, for example, as the emissivity increases from 0.05 to 0.45, the peak channel temperature

(at entry as well as exit) decreases by 34.23%, while a further increase in emissivity to 0.85 brings down T_{max} by an additional 18.02%.

Figure 3 shows the local left and right wall temperature profiles for three different values of convection heat transfer coefficient, $h = 5$, 25, and $100\,W/m^2K$, respectively, to study the effect of regimes of convection (free or forced) on temperature distribution. The value of $h = 5\,W/m^2K$ implies free-convection-dominant regime, while $h = 100\,W/m^2K$ signifies forced-convection-dominant regime. It may be seen that temperature profiles pertaining to the left wall remain essentially similar to those in Figure 2, with the temperature at a given location of the left wall decreasing as one moves toward larger values of convection heat transfer coefficient, obviously because of increase in the rate of heat transfer by convection. Further, the degree of decrease of local left wall temperature is quite large between $h = 5$ and $25\,W/m^2K$, while that between $h = 25$ and $100\,W/m^2K$ is not as pronounced as above. This is because one is already in forced-convection-dominant regime beyond $h = 25\,W/m^2K$. To quantify, T_{max} in the channel drops down by 55.12% as h rises from 5 to $25\,W/m^2K$, while it further drops to a lesser extent by only 49.27% as h subsequently rises from 25 to $100\,W/m^2K$. With regard to the right wall, Figure 3 reveals a trend just the reverse of what has been noticed in Figure 2. That is, the

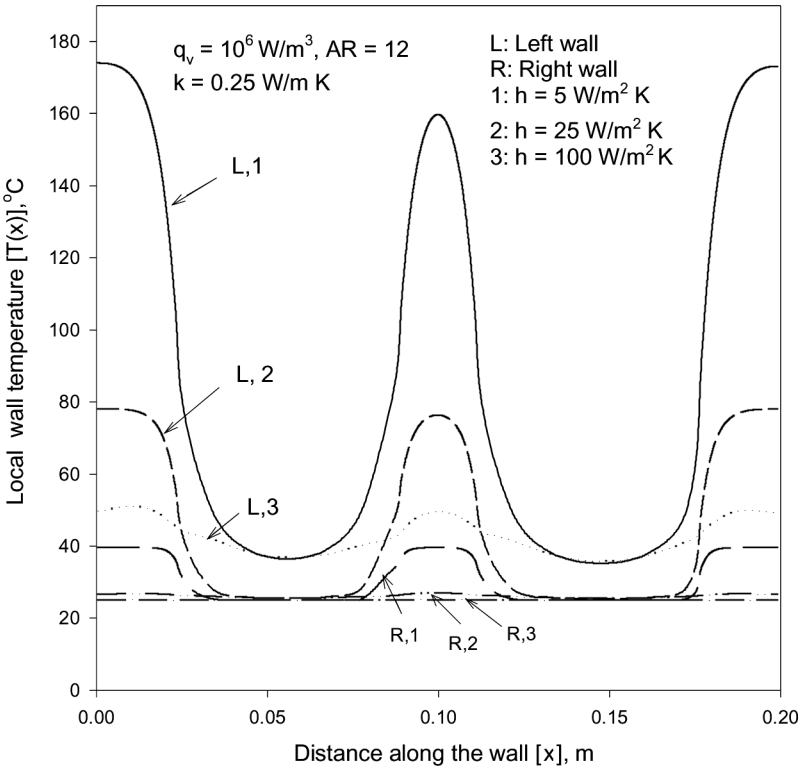

Figure 3. Variation of local temperature along the left and right channel walls in different regimes of convection.

temperature change along the right wall becomes less apparent toward larger values of h. The reason for this could be attributed to the following. The right wall does not have any heat source. Any rise in its temperature, in the present problem, is owing to the heat it receives by radiation from the left wall. Since, toward larger values of h, most of the heat dissipation from the left wall occurs by convection, not much is directed to the right wall by radiation. Thus perceptible changes in the right wall temperature start diminishing toward larger values of h.

Local temperature distribution along the left and right walls of the channel, for $q_v = 10^6\,\mathrm{W/m^3}$, $e = 0.45$, AR $= 12$, and $h = 5\,\mathrm{W/m^2\,K}$, and for three typical values of thermal conductivity, $k = 0.25$, 1, and $10\,\mathrm{W/m\,K}$, is depicted in the family of six curves shown in Figure 4. As in Figure 3, here too, there is a monotonic drop in temperature at a given location with increase in thermal conductivity for the left and right walls of the channel, with other parameters held fixed. So far as individual temperature profiles are concerned, the nature of temperature variation is just similar to that in Figures 2 and 3, though for the case with $k = 10\,\mathrm{W/m\,K}$, in the non-heat portion in the left wall, the temperature is almost constant, rendering those portions isothermal. The figure shows that $T_{\max}$ decreases by 11.96% with k increasing from 0.25 to $1\,\mathrm{W/m\,K}$, while the drop in $T_{\max}$ is as much as 49.87% for subsequent increase of k from 1 to $10\,\mathrm{W/m\,K}$.

Figure 5 shows the left and right wall temperature profiles, for $q_v = 10^6\,\mathrm{W/m^3}$, $k = 0.25\,\mathrm{W/m\,K}$, $e = 0.45, h = 5\,\mathrm{W/m^2\,K}$, and for five different aspect ratios,

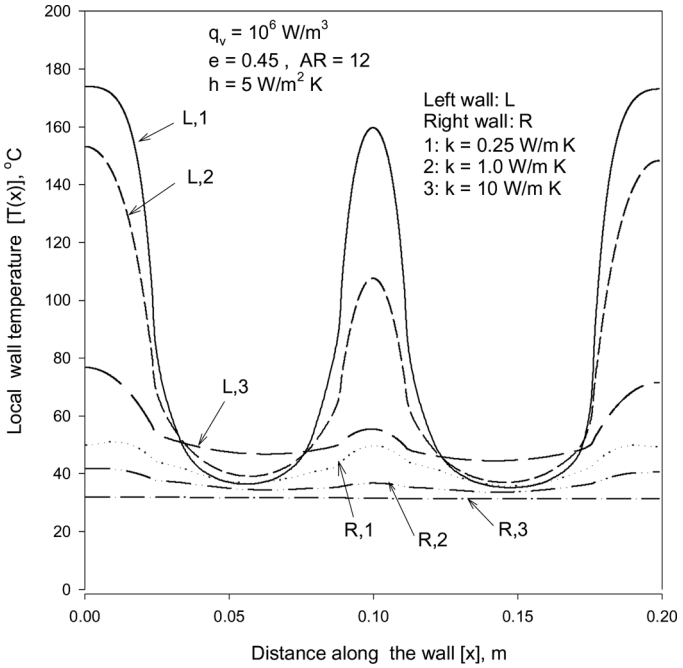

Figure 4. Variation of local temperature along the left and right channel walls for different thermal conductivities.

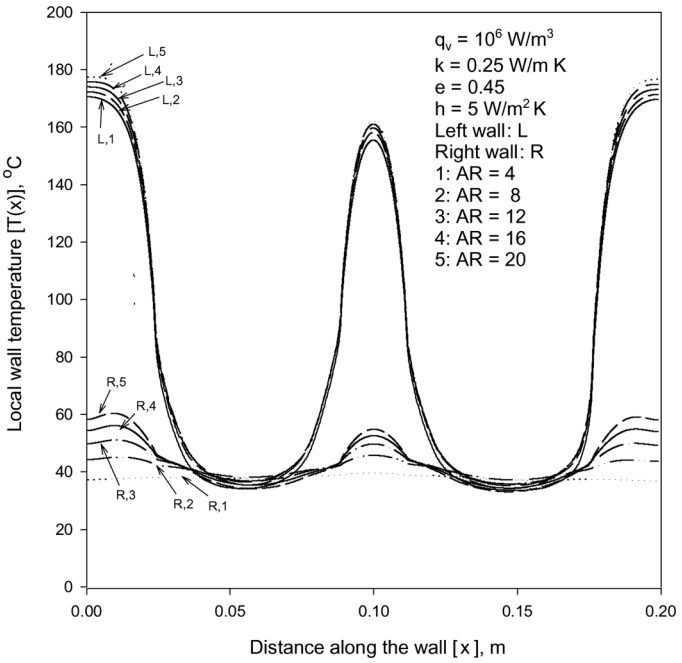

Figure 5. Variation of local temperature along the left and right channel walls for different aspect ratios.

AR = 4, 8, 12, 16, and 20. As may be seen, with an increase in aspect ratio, as the walls of the channel come closer together, the access for the heat generating left wall to the top and bottom free (open) boundaries comes down. At the same time, the rate at which the right wall receives heat by radiation from the left wall increases. The net result of the two is noticed in Figure 5, with the right wall experiencing comparatively significant rise in its temperature with increasing aspect ratio, while for the left wall, the rise in temperature is not that significant. For example, in the case chosen for discussion in Figure 5, at the channel entry, the right wall temperature is increasing by 56.25% as the AR increases from 4 to 20, while the left wall temperature at the same location (i.e., the channel entry) increases by only 3.99% for the same increase in aspect ratio.

Variation of Maximum Temperature in the Channel

Since the minimization of the peak channel temperature ($T_{\max}$) helps in controlling the entire channel temperature as well, a study of the variation of the maximum channel temperature with reference to various pertinent parameters is taken up in this section.

Figure 6 narrates the variation of $T_{\max}$ with surface emissivity e of the channel wall, for four typical values of $h = 5$, 10, 15, and 25 $\mathrm{W/m^2\,K}$), and for a fixed set of other parameters, namely, $q_v = 10^6\,\mathrm{W/m^3}$, AR = 12, and $k = 1\,\mathrm{W/m\,K}$. The figure shows that there is a monotonic decrease in $T_{\max}$ with increase in emissivity e for a

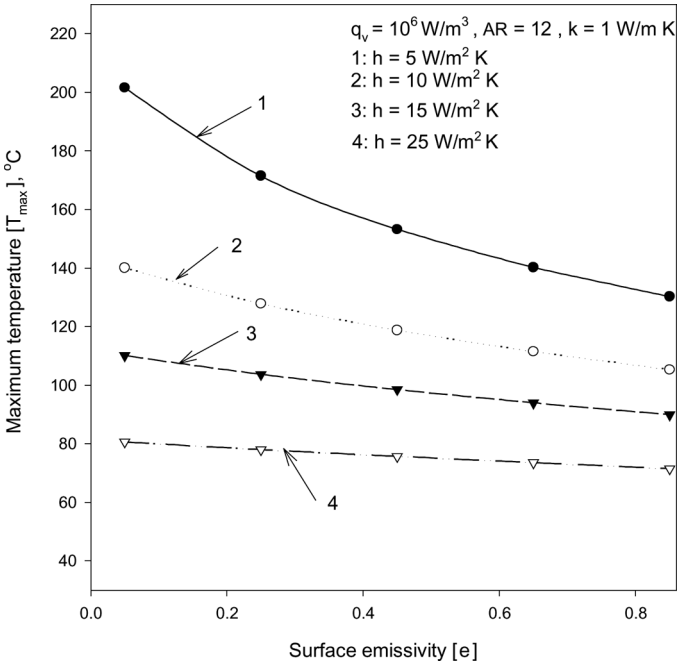

Figure 6. Variation of maximum channel temperature with surface emissivity in different regimes of convection.

given heat transfer coefficient h and also with increase in h for a given e. The above is understandable because the rates of heat dissipation by convection and radiation show a direct proportionality with h and e, respectively. The figure also highlights the role of surface radiation in the free-convection-dominant regime. For example, for $h = 5$ W/m^2 K, T_{max} undergoes a larger drop, by 35.41%, as e increases from 0.05 to 0.85, while it decreases by a meager 11.31% for the same rise in e in the forced-convection-dominant regime ($h = 25$ W/m^2 K).

Figure 7 provides a family of three curves showing the variation of T_{max} with convection heat transfer coefficient h, drawn for three values of k, viz., 0.25, 0.5, and 1 W/m K, for a fixed set of other parameters ($q_v = 10^6$ W/m^3, AR = 12, and $e = 0.45$). The figure clearly shows that the thermal conductivity of the board shows reasonable effect on T_{max} in the free-convection-dominant regime. However, the role of k starts diminishing as one moves toward the regime of forced-convection dominance. Here, convection heat transfer coefficient, and thus the rate of convection heat transfer, dominates conduction, and thus, with other parameters held fixed, T_{max} does not undergo substantive variation with k, rendering the curves to almost merge with each other beyond $h = 50$ W/m^2 K. For example, in the case taken up here, as k increases from 0.25 to 1 W/m K, T_{max} decreases by 11.96% at $h = 5$ W/m^2 K, while it comes down by only 0.73% at $h = 50$ W/m^2 K.

The variation of T_{max} with surface emissivity e for three values of k (=0.25, 0.5 and 1 W/m K) and fixed values of other parameters ($q_v = 10^6$ W/m^3, AR = 12, and $h = 5$ W/m^2 K) is shown in Figure 8. The figure clearly explains the interaction

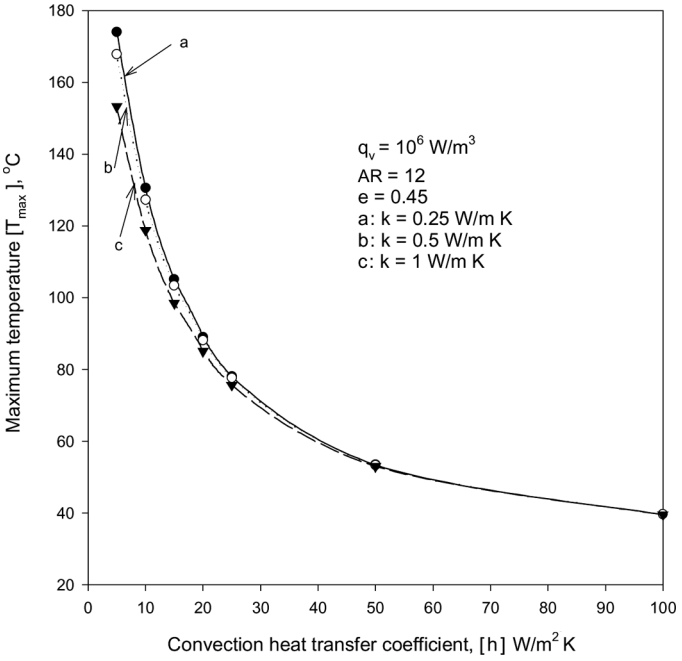

Figure 7. Variation of maximum channel temperature with convection heat transfer coefficient for different thermal conductivities.

between conduction and surface radiation for a given regime of convection (i.e., a given value of heat transfer coefficient h). It may be seen that, for a given k, there is a steep drop in $T_{\max}$ as e increases from 0.05 to 0.45, while the role of radiation is less pronounced toward larger values of e. For example, in the present case, for $k = 0.25\,\mathrm{W/m\,K}$, $T_{\max}$ is found to be decreasing by as much as 33.96% as the coating of the board is changed from a poor emitter ($e = 0.05$) to a moderate emitter ($e = 0.45$). For a subsequent change in the surface to a good emitter ($e = 0.85$), $T_{\max}$ comes down by only 17.14%. In addition to this, the figure also reveals a monotonic drop in $T_{\max}$ with k, for a given e.

Figure 9 describes the nature of variation of $T_{\max}$ with aspect ratio for three typical surface coatings of the walls of the channel ($e = 0.05$, 0.45, and 0.85), for $q_v = 10^6\,\mathrm{W/m^3}$, $k = 0.25\,\mathrm{W/m\,K}$, and $h = 5\,\mathrm{W/m^2\,K}$. For a given e and other parameters held fixed as above, $T_{\max}$ seems to be increasing only mildly with aspect ratio. However, the aspect ratio effect on $T_{\max}$ is marginally better toward larger values of e. In the present case, for $e = 0.05$, $T_{\max}$ is seen to be increasing by only 0.43% as AR increases from 4 to 20. In contrast, for $e = 0.85$, $T_{\max}$ is increasing by a relatively larger 7.07%. The figure further shows that, for a given AR, there is a significant drop in $T_{\max}$ as e increases from 0.05 to 0.45, while the degree of decrease of $T_{\max}$ is less significant as e further increases to 0.85. In the present case, for AR = 12, $T_{\max}$ decreases by 34.23% as e rises from 0.05 to 0.45, and by only 18.02% as e further increases to 0.85.

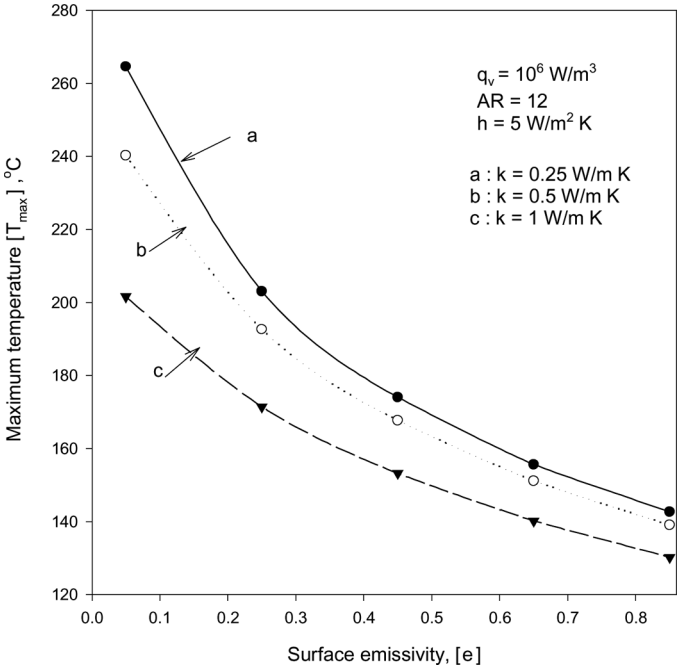

Figure 8. Variation of maximum channel temperature with surface emissivity for different thermal conductivities.

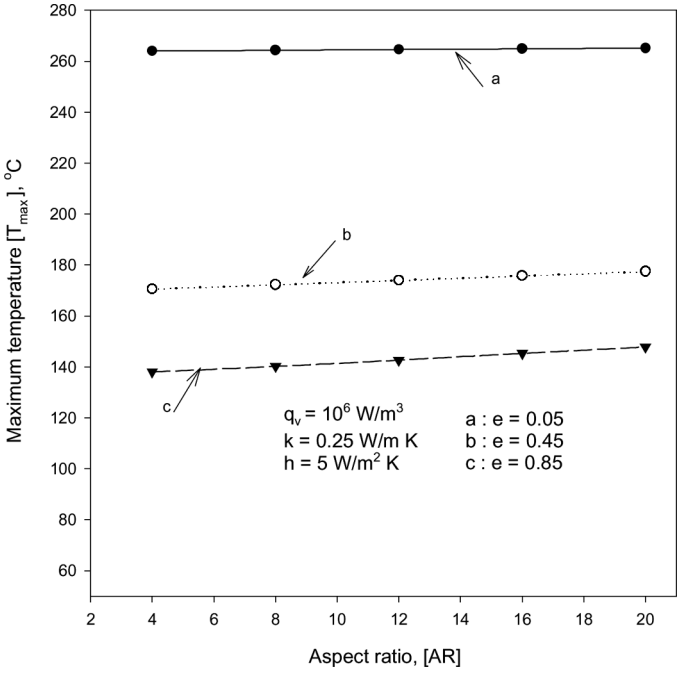

Figure 9. Variation of maximum channel temperature with aspect ratio for different surface emissivities.

Relative Roles of Convection and Radiation in Heat Dissipation from the Channel

Figure 10 shows the relative contributions of convection and radiation to channel heat dissipation as a function of aspect ratio for three different values of convection heat transfer coefficient, $h = 5$, 10, and $25\,\mathrm{W/m^2\,K}$. The study is performed for fixed values of other parameters, namely, $q_v = 10^6\,\mathrm{W/m^3}$, $k = 0.25\,\mathrm{W/m\,K}$ and $e = 0.85$. For each value of h, the figure shows a pair of curves, one pertaining to convection and the other to radiation. The figure shows that, for a given h, the contribution of convection to heat dissipation increases with AR, while its radiation counterpart shows a mirror-image variation. The figure shows the interesting fact that the curves pertaining to convection and radiation heat transfer, in the free-convection-dominant regime of $h = 5\,\mathrm{W/m^2\,K}$, cross each other for an aspect ratio between 1.5 and 2, indicating equal contributions from each of the two modes for that aspect ratio. The figure further reveals the importance of radiation in carrying the mandated heat load in all regimes of convection, more so in the free-convection-dominant regime. It is pertinent to note that even in the forced-convection-dominant regime, radiation can contribute to heat dissipation by as much as 15% toward smaller values of aspect ratio.

Figure 11 shows the relative contributions of convection and radiation to channel heat dissipation, plotted against surface emissivity e, for $h = 5$, 10, and $25\,\mathrm{W/m^2\,K}$, while the other parameters, namely, $q_v = 10^6\,\mathrm{W/m^3}$, $k = 0.25\,\mathrm{W/m\,K}$, and AR = 10, are held fixed. The figure shows the effect of surface coating provided

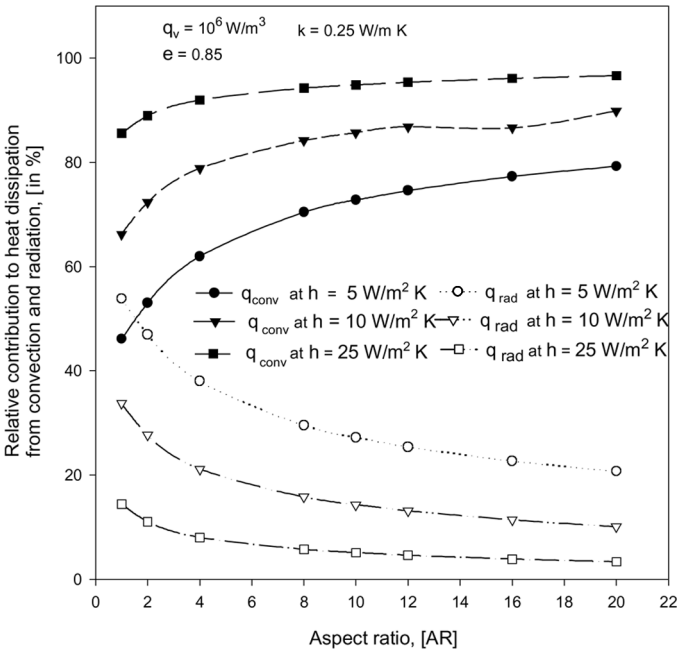

Figure 10. Relative contributions of convection and radiation to channel heat dissipation with aspect ratio in different regimes of convection.

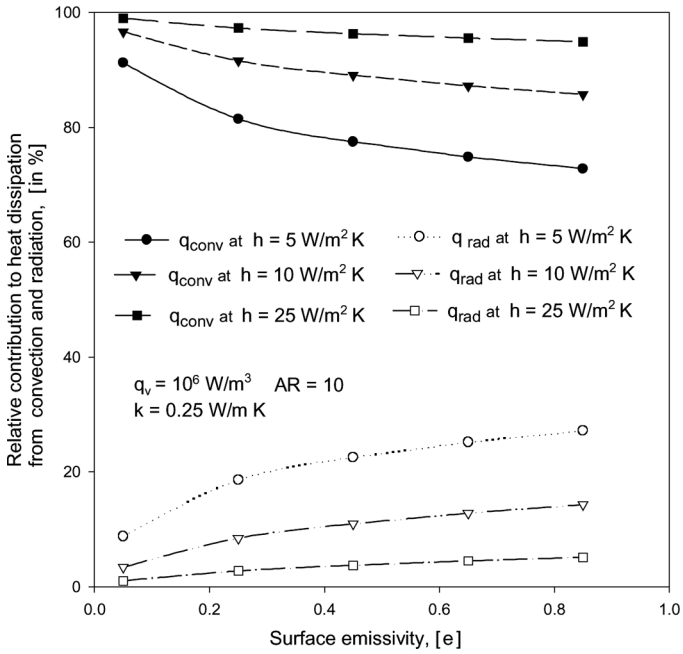

Figure 11. Relative contributions of convection and radiation to channel heat dissipation with surface emissivity in different regimes of convection.

on the walls of the channel on heat dissipation in various regimes of convection. It may be seen that, as the surface coating of the walls is changed from a poor emitter (such as highly polished aluminum sheet, with $e = 0.05$) to a good emitter (such as black paint, with $e = 0.85$), the contribution from radiation increases significantly in all three regimes of convection considered for study. The above effect is more pronounced in the free-convection-dominant regime ($h = 5\,\mathrm{W/m^2\,K}$), wherein the radiation contribution goes up to about 30% from about 10% as e increases from 0.05 to 0.85. It is to be remembered that the above plot is for the aspect ratio of 10, and the surface emissivity effect could have been much more had the plot been drawn for a lower value of aspect ratio. The figure also reiterates the observation made with regard to Figure 9 that the optimum for e hovers around 0.45 for the problem taken up in the present study.

CONCLUDING REMARKS

A fundamental numerical study of the problem of conjugate convection with surface radiation from a vertical, parallel-plate, channel provided with three flush-mounted discrete heat sources in its left wall has been made. The effects of all governing parameters on several important results have been clearly elucidated. It has been seen that the effect of surface radiation in problems of this class cannot be overlooked in any regime of convection, more so if one is working in a free-convection-environment. It has also been noticed that long narrow channels are unadvisable in

comparison to relatively short, broadly spaced channels. The studies also revealed that effective control of heat dissipation, and thus the peak channel temperature, is possible by just changing the surface coating of the board from a poor emitter to a good emitter, even when one has no control over other parameters involved in the problem.

REFERENCES

1. A. E. Zinnes, The Coupling of Conduction with Laminar Natural Convection from a Vertical Flat Plate with Arbitrary Surface Heating, *ASME J. Heat Transfer*, vol. 92, pp. 528–534, 1970.
2. S. S. Tewari and Y. Jaluria, Mixed Convection Heat Transfer from Thermal Sources Mounted on Horizontal and Vertical Surfaces, *ASME J. Heat Transfer*, vol. 112, pp. 975–987, 1990.
3. M. A. Gorski and O. A. Plumb, Conjugate Heat Transfer from an Isolated Heat Source in a Plane Wall, *Proc. Winter Annual Meeting of the American Society of Mechanical Engineers*, ASME HTD-210, pp. 99–105, 1992.
4. K. Kishinami, H. Saito, and J. Suzuki, Combined Forced and Free Laminar Convective Heat Transfer from a Vertical Plate with Coupling of Discontinuous Surface Heating, *Int. J. Numer. Meth. Heat Fluid Flow*, vol. 5, pp. 839–851, 1995.
5. K. D. Cole, Conjugate Heat Transfer from a Small Heated Strip, *Int. J. Heat Mass Transfer*, vol. 40, pp. 2709–2719, 1997.
6. F. Mendez and C. Trevino, The Conjugate Conduction-Natural Convection Heat Transfer along a Thin Vertical Plate with Non-uniform Internal Heat Generation, *Int. J. Heat Mass Transfer*, vol. 43, pp. 2739–2748, 2000.
7. A. A. Dehghan and M. Behnia, Combined Natural Convection-Conduction and Radiation Heat Transfer in a Discretely Heated Open Cavity, *ASME J. Heat Transfer*, vol. 118, pp. 56–64, 1996.
8. C. Gururaja Rao, C. Balaji, and S. P. Venkateshan, Numerical Study of Laminar Mixed Convection from a Vertical Plate, *Int. J. Transport Phenomena*, vol. 2, pp. 143–157, 2000.
9. C. Gururaja Rao, C. Balaji, and S. P. Venkateshan, Conjugate Mixed Convection with Surface Radiation from a Vertical Plate with a Discrete Heat Source, *ASME J. Heat Transfer*, vol. 123, pp. 698–702, 2001.
10. C. Gururaja Rao, C. Balaji, and S. P. Venkateshan, Effect of Surface Radiation on Conjugate Mixed Convection in a Vertical Channel with a Discrete Heat Source in Each Wall, *Int. J. Heat Mass Transfer*, vol. 45, pp. 3331–3347, 2002.
11. C. Gururaja Rao, C. Balaji, and S. P. Venkateshan, Conjugate Mixed Convection with Surface Radiation in a Vertical Channel with Symmetric and Uniform Wall Heat Generation, *Int. J. Transport Phenomena*, vol. 5, pp. 75–101, 2003.
12. C. Gururaja Rao, A. Venkata Krishna, and P. Naga Srinivas, Simulation Studies on Multi-mode Heat Transfer from a Square-Shaped Electronic Equipment with Multiple Discrete Heat Sources, *Numer. Heat Transfer A*, vol. 48, pp. 427–446, 2005.
13. C. Gururaja Rao, Buoyancy-Aided Mixed Convection with Conduction and Surface Radiation from a Vertical Electronic Board with a Traversable Discrete Heat Source, *Numer. Heat Transfer A*, vol. 45, pp. 935–956, 2004.
14. C. Gururaja Rao, Numerical Study of Mixed Convection and Surface Radiation in a Vertical Channel, *SSME J. Mech. Eng.*, vol. 6, pp. 45–54, 2002.
15. N. Bianco, L. Langellotto, O. Manca, and V. Naso, Numerical Analysis of Radiative Effects on Natural Convection in Vertical Convergent and Symmetrically Heated Channels, *Numer. Heat Transfer A*, vol. 49, pp. 369–391, 2006.

16. K. Slimi, L. Zili-Ghedira, S. Ben Nasrallah, and A. A. Mohamad, A Transient Study of Coupled Natural Convection and Radiation in a Porous Vertical Channel Using the Finite-Volume Method, *Numer. Heat Transfer A*, vol. 45, pp. 451–478, 2004.
17. M. N. Borjini, C. Mbow, and M. Daguenet, Numerical Analysis of the Effect of Radiation on Laminar Steady Natural Convection in a Two-Dimensional Participating Medium between Two Horizontal Confocal Elliptical Cylinders, *Numer. Heat Transfer A*, vol. 35, pp. 467–494, 1999.
18. P. F. Hsu and Z. Tan, Radiative and Combined-Mode Heat Transfer within L-Shaped Nonhomogeneous and Nongray Participating Media, *Numer. Heat Transfer A*, vol. 31, pp. 819–835, 1997.
19. C. I. Baek, K. S. Lee, and W. S. Kim, Study of Combined Heat Transfer in a Three Dimensional Enclosure with a Protruding Heat Source, *Numer. Heat Transfer A*, vol. 32, pp. 733–747, 1997.
20. K. H. Lee, J. S. Lee, and M. Choi, Parametric Analysis of Radiative-Convective Heat Transfer around a Circular Cylinder in a Cross Flow Using the Finite Volume Radiation Solution Method, *Numer. Heat Transfer A*, vol. 29, pp. 181–196, 1996.
21. R. Siegel and J. R. Howell, *Thermal Radiation Heat Transfer*, Taylor & Francis, Washington and London, 1992.
22. H. C. Hottel, Radiant Heat Transmission, in W. H. McAdams (ed.), *Heat Transmission*, 3rd ed., McGraw-Hill, New York, 1954.